Heat transfer in the flow of a cold, two-dimensional vertical liquid jet against a hot, horizontal plate

Shu, Jian Jun; Wilks, Graham

1996

Shu, J. J., & Wilks, G. (1996). Heat transfer in the flow of a cold, two-dimensional vertical liquid jet against a hot, horizontal plate. International Journal of Heat and Mass Transfer, 39(16), 3367-3379.

https://hdl.handle.net/10356/93926

https://doi.org/10.1016/0017-9310(96)00020-8

Heat transfer in the flow of a cold, two-dimensional vertical liquid jet against a hot, horizontal plate

JIAN-JUN SHU[a], *GRAHAM WILKS*[b1]

[a]*Department of Applied Mathematical Studies, University of Leeds, Leeds LS2 9JT, England, U.K.*

[b]*Department of Mathematics, University of Keele, Keele, Staffordshire ST5 5BG, England, U.K.*

Abstract

A cold, thin film of liquid impinging on an isothermal hot, horizontal surface is modelled as a two-dimensional jet of prescribed uniform velocity, film thickness and temperature. An approximate solution for the velocity and temperature distributions in the flow along the horizontal surface is developed, which exploits the Watson hydrodynamic similarity solution for thin film flow. A numerical solution of high accuracy has also been obtained. Comparisons indicate that the approximate solution may provide a valuable basis for assessing flow and heat transfer in more complex settings modelled by jet impingement such as cylinder inundation flows.

1. INTRODUCTION

In response to the abundance of practical applications the heat transfer associated with impinging jets has been the subject of numerous theoretical and experimental research studies reported in the literature. In particular the heat transfer effected by the steady flow of a circular free jet against plane surfaces has been discussed by a number of authors [1-6]. The seminal paper by Watson [7] on the radial spread of a liquid jet over a horizontal plane has frequently been instrumental in framing the hydrodynamic background to such studies. In the same paper, Watson also presents a discussion of the flow field associated with a vertical two-dimensional jet striking a horizontal surface. Its relevance to practical circumstances is not quite as immediately obvious. However, the inundation and drainage film flow between vertically adjacent horizontal cylinders has long been recognized as an important element in the heat exchange process as utilized in a variety of industrial settings. This is particularly true in the context of condensers, as used in power generation. Here the draining fluid is accumulated condensate. The assessment of heat transfer characteristics in such settings is based on Nusselt theory. Unfortunately the absence of inertia in the theory leads to the prediction of zero heat transfer at the upper generator of an inundated cylinder. The work that follows in part addresses this

[1] Author to whom correspondence should be addressed.

inconsistency. If the inundating film is modelled as an impinging two-dimensional jet it is noteworthy that Watson's work on the plane jet may be exploited to advantage in these circumstances also, particularly if the film thickness to cylinder radius ratio is small. For then, on a length scale typical of the width of the draining film the cylinder surface at impingement may be regarded as locally flat. Accordingly, further insight into the flow and heat transfer characteristics near the top of an inundated cylinder may usefully be obtained by examining in the first instance the heat transfer features of the two dimensional jet flow against a plane, horizontal surface. Moreover, any underlying methodology of solution may indicate how best to incorporate inertia into a detailed assessment of the heat transfer characteristics of inundation and drainage flow over a cylinder. Current analyses of such flows [8-11] fail to distinguish between the effects of a thin, high speed jet as compared to a thick, low speed jet when each give rise to a common flow rate. By demonstrating that the heat transfer from an inundated cylinder is dependent upon the spacing between vertically adjacent tubes, Mitrovic [12] indicates that such a distinguishing capability in theoretical models is called for. Some progress has been made in the hydrodynamic context. Depending upon the precise impingement conditions a variety of film thickness profiles associated with a common flow rate has been demonstrated in Abdelghaffer *et al.* [13].

NOMENCLATURE

C_p	specific heat
(f, u, v, ϕ, w)	dependent variables
f_0, ϕ_0	initial profiles
H, h	film thicknesses
H_0	jet semi-thickness
k	thermal conductivity
l	leading edge shift constant
Nu	Nusselt number
Pr	Prandtl number
Q	$U_0 H_0$
q	heat flux
Re	Reynolds number
T	temperature
T_0	jet temperature
T_w	plate temperature
U_0	jet velocity
U_s	free surface velocity
$\mathbf{V} = (U, V)$	velocity and its components
(X, Y), (x, y)	Cartesian coordinates measured along and normal to the plate
x_0, x_1	ends of Regions 1 and 2.

Greek symbols

β	dimensionless free surface temperature
Γ	Gamma function
Δ	δ_T/δ
δ, δ_T	dimensionless boundary layer thicknesses of velocity and temperature variations
η_T	η/Δ
κ	thermometric conductivity
μ, ν	dynamic and kinematic viscosities
(ξ, η)	dimensionless coordinates
ρ	density
τ	skin friction
ψ	stream function.

Subscripts

w	Watson.

Superscript

$^-$	dimensional analysis.

In the work that follows, it is once again indicated how Watson's hydrodynamic theory can be exploited to great advantage in the heat transfer analysis of the film cooling accompanying the spread of a cold, two-dimensional jet against a hot, horizontal plate. An approximate solution scheme is developed which incorporates the idealized notions of viscous and thermal penetration of the free surface, before downstream asymptotic similarity solutions apply. A judicious combination of momentum integral and similarity methods provides comprehensive estimates of the impingement flow and heat transfer

characteristics. To assess the viability of the solution scheme, as a prelude to cylinder inundation analysis, a full numerical solution is also obtained. A high level of agreement between the two solutions is demonstrated.

2. MODELLING AND BASIS OF APPROXIMATE SOLUTION

The problem to be examined concerns the film cooling which occurs when a cold vertically draining sheet strikes a hot horizontal plate. Although a sheet of fluid draining under gravity will accelerate and thin, at impact it is reasonable to model the associated volume flow as a jet of uniform velocity U_0 and semi-thickness H_0 , as illustrated in Fig. 1. The notation $Q = U_0 H_0$ is introduced for the flow rate and a film Reynolds number may be defined as $Re = Q/v$, where v is the kinematic viscosity of the fluid. The underlying hydrodynamics of the fluid flow may be inferred from Watson [7], who was principally concerned with the radial spread of an axi-symmetric liquid jet over a horizontal plane.

They may be summarized as:

(i) a deeply imbedded stagnation boundary layer of thickness $O(v H_0/U_0)^{1/2}$;
(ii) an outer viscid deflection region of $O(H_0)$, in which fluid rapidly accelerates from the value zero on the axis of symmetry to the free stream value $O(U_0)$;
(iii) a Blasius region at distances greater than $O(H_0)$ from the axis of symmetry in which a boundary layer develops against the plane, effectively within a uniform stream ;
(iv) a transition region in which viscous effects penetrate the free surface and reduce its velocity ;
(v) a region well away from the axis of symmetry where similarity solutions for the developing film thickness, the free surface velocity and the velocity distribution can be found.

Watson also recognized the eventual termination of the flow regime by a hydraulic jump. Since the objective here is ultimately to develop a methodology for the flow around a cylinder where no such phenomenon is observed, the associated complications of a possible hydraulic jump will not be considered.

The temperature condition within which heat transfer estimates will be obtained assumes a constant temperature T_w. at the plane and zero heat flux at the free surface. If water is the coolant medium then it has to be noted that the rates of viscous and thermal diffusion will be appreciably different. The rate of viscous diffusion will exceed that of temperature diffusion. The point at which viscous effects penetrate the free surface will therefore occur before the point at which the free surface first experiences the presence of the hot plane. This physical appraisal of the developing flow field provides the framework for the initial approximate method of solution. Schematically the flow may be represented as in Fig. 2 and divided into the following regions.

Region 1

In this region the impinging jet essentially experiences an inviscid symmetric division and deflection through 90 º. For high flow rates the deeply imbedded stagnation boundary layer is $O(\nu H_0/U_0)^{1/2}$, i.e. $O(H_0 Re^{-1/2})$ and as a first approximation or in the limit of large *Re* may be regarded as negligibly small. A viscous boundary layer develops against the horizontal plate within the deflected jet and eventually penetrates the free surface marking the end of Region 1. A thermal boundary layer develops simultaneously, but for Prandtl numbers greater than unity this will still be evolving at the end of Region 1.

Region 2

A judicious choice of approximating profiles in Region 1 is designed to approximate immediate transition to the film similarity solution at the onset of Region 2. Consequently Region 2 is examined under the assumption that the full hydrodynamic similarity solution is applicable. The adjustment of the temperature field as thermal effects develop and penetrate the free surface within this hydrodynamic setting is monitored. The end of Region 2 is notionally reached when the presence of the hot wall is first detected at the free surface.

Region 3

In the film cooling setting, when there is zero heat flux at the free surface, the film will eventually reach a uniform temperature distribution, coinciding with the temperature of the wall. Again within the established hydrodynamics, Region 3 covers the evolution towards this asymptotic state once the wall temperature effects penetrate the free surface.

3. **GOVERNING EQUATIONS**

The flow under investigation has been modelled as a steady, two-dimensional flow of incompressible fluid. In the absence of body forces external pressure gradients and viscous dissipation the equations expressing conservation of mass, momentum and energy are consequently

$$\nabla \cdot \mathbf{V} = 0 \qquad (1)$$

$$\rho(\mathbf{V} \cdot \nabla)\mathbf{V} = \mu \nabla^2 \mathbf{V} \qquad (2)$$

$$\rho C_p(\mathbf{V} \cdot \nabla) T \simeq k \nabla^2 T. \qquad (3)$$

In the specified physical setting, the equations are to be solved subject to the following conditions :

$$U = V = 0 \quad T = T_w \quad \text{on } Y = 0, X \geqslant 0 \qquad (4)$$

$$\frac{\partial U}{\partial Y} = 0 \quad \frac{\partial T}{\partial Y} = 0 \quad \text{at } Y = H(X), X \geqslant 0 \qquad (5)$$

$$\int_0^{H(X)} U(X, Y)\, \mathrm{d}Y = \text{constant} = H_0 U_0 \quad \text{for } X \geqslant 0. \qquad (6)$$

On the assumption that the film thickness remains thin relative to a characteristic horizontal dimension, a boundary layer treatment of the equations leads to significant simplification.

The following nondimensional variables are introduced

$$x = \frac{X}{ReH_0} \quad u = \frac{Y}{H_0} \quad \bar{h}(x) = \frac{H(X)}{H_0}$$

$$\bar{U} = \frac{U}{U_0} \quad \bar{V} = \frac{ReV}{U_0} \quad \bar{\phi} = \frac{T - T_w}{T_0 - T_w}. \qquad (7)$$

In the limit $Re \to +\infty$, with x remaining O(1), the following equations are obtained :

$$\frac{\partial \bar{U}}{\partial x} + \frac{\partial \bar{V}}{\partial y} = 0 \qquad (8)$$

$$\bar{U}\frac{\partial \bar{U}}{\partial x} + \bar{V}\frac{\partial \bar{U}}{\partial y} = \frac{\partial^2 \bar{U}}{\partial y^2} \qquad (9)$$

$$Pr\left(\bar{U}\frac{\partial \bar{\phi}}{\partial x} + \bar{V}\frac{\partial \bar{\phi}}{\partial y}\right) = \frac{\partial^2 \bar{\phi}}{\partial y^2}, \qquad (10)$$

where $Pr = \nu/\kappa$ is the Prandtl number.

The boundary conditions now read

$$\bar{U} = \bar{V} = 0 \quad \bar{\phi} = 0 \quad \text{on } y = 0 \quad x \geqslant 0 \qquad (11)$$

$$\frac{\partial \bar{U}}{\partial y} = 0 \quad \frac{\partial \bar{\phi}}{\partial y} = 0 \quad \text{at } y = \bar{h}(x) \quad x \geqslant 0 \qquad (12)$$

$$\int_0^{\bar{h}(x)} \bar{U}\, \mathrm{d}y = 1 \quad \text{for } x \geqslant 0. \qquad (13)$$

These have been quoted in the context of the fully developed film flow field which is approached in Region 3. Equations (8) and (9), under the hydrodynamic boundary conditions, have been shown by Watson [7] to possess similar solutions. A simple supplementary thermal solution of uniform temperature is also present. These solutions provide the basis for developing comprehensive approximate solutions for the complete

flowfield downstream of the symmetry point of impingement incorporating Regions 1, 2 and 3.

4. DOWNSTREAM SIMILARITY SOLUTIONS

Introducing a similarity variable $\eta = y/\,h(x)$, a stream function form of solution $\psi(x, y) = \bar{U}_s(x)\bar{h}(x)f(\eta)$ leads to the Watson similarity solution as the solution of

$$2f''' + 3c^2 f'^2 = 0 \quad f'(0) = 0 \quad f'(1) = 1 \quad f''(1) = 0. \tag{14}$$

Here $\bar{U}_s(x)$ represents the nondimensional unknown velocity at the free surface and c can be obtained analytically as

$$\frac{\Gamma(\frac{1}{3})\Gamma(\frac{1}{2})}{3\Gamma(\frac{5}{6})} \approx 1.402.$$

Together with the numerical solution of equation (14), the hydrodynamics are fully determined by the results

$$\bar{U}_s(x) = \frac{9c^2}{2\pi^2(x+l)} \quad \bar{h}(x) = \frac{\pi}{\sqrt{3}}(x+l). \tag{15}$$

Here l is a nondimensional shift constant reflecting that the solutions hold at large distances from the jet incidence. In due course l may be estimated by further consideration of the boundary layer growth from the point of impact of the jet.

With $\bar{\phi}(x, y) = \bar{\phi}(\eta)$ it is readily shown that $\bar{\phi}$ satisfies

$$\bar{\phi}'' = 0 \quad \bar{\phi}(0) = \bar{\phi}'(1) = 0. \tag{16}$$

Thus, as anticipated, the asymptotic downstream solution for the temperature distribution is just $\bar{\phi}(\eta) = 0$, i.e. the temperature T_w ultimately persists throughout the film if $\partial T/\partial y = 0$ at the free surface.

5. APPROXIMATE SOLUTIONS

An approximate solution scheme is now presented which examines closely the flow at impingement. The solution is built up from this vicinity, stage by stage, to provide comprehensive details of the velocity and temperature distribution along the entire plate.

5.1. Region 1

At impact, an inviscid deflection of the draining sheet occurs over a negligibly small length scale. Essentially the flow along the plane in this region is modelled as a

horizontal film of uniform velocity U_0 arriving at the leading edge $X = 0$ of a semi-infinite flat plate. Only after deflection will the flow be aware of the presence of the solid boundary, and only then will viscous effects begin to influence the flow field. The development of a viscous boundary layer within a uniform velocity film indicates a close parallel in this region with the Blasius boundary layer flow. Similarly the temperature differential between the plane and the fluid will only begin to influence the temperature distribution after deflection. Thus, a developing thermal boundary layer may also be anticipated from $X = 0$.

The equations governing the viscous and thermal boundary layers are exactly the same as equations (8)−(10), but the boundary conditions now read

$$\bar{U} = 0, \bar{V} = 0, \bar{\phi} = 0 \quad \text{on } y = 0, x \geqslant 0 \quad \bar{U} \to 1, \bar{\phi} \to 1$$

as y approaches the outer limits of the viscous and thermal boundary layers respectively

$$\bar{U} = 1, \bar{\phi} = 1 \quad \text{at } x = 0, y > 0.$$

The transformations

$$\psi(x, y) = (2x)^{1/2} \bar{f}(\bar{\eta}), \quad \bar{\phi}(x, y) = \bar{\phi}(\bar{\eta}), \quad \bar{\eta} = \frac{y}{(2x)^{1/2}} \tag{17}$$

lead to

$$\bar{f}''' + \bar{f}\bar{f}'' = 0 \quad \bar{f}(0) = \bar{f}'(0) = 0 \quad \bar{f}'(\bar{\eta}) \to 1 \quad \text{as } \bar{\eta} \to +\infty$$

$$\frac{1}{Pr}\bar{\phi}'' + \bar{f}\bar{\phi}' = 0, \quad \bar{\phi}(0) = 0 \quad \bar{\phi}(\bar{\eta}) \to 1 \quad \text{as } \bar{\eta} \to +\infty. \tag{18}$$

These equations, as anticipated, are the well documented forced convection boundary layer equations. Their solutions for $Pr > 1$ indicate that the length scale of thermal diffusion can be significantly less than that of viscous diffusion.

Viscous effects, in due course, must penetrate the free surface and the transition region of Fig. 1 is essentially a region of adjustment from the Blasius profile to the Watson similarity profile. As the profiles are not greatly dissimilar, a device which in effect compresses the transition region to a single point is introduced. An approximate velocity profile

$$\bar{U}(x, y) = \bar{U}_s(x) f'\left(\frac{y}{\delta}\right), \quad \eta = \frac{y}{\delta(x)} \tag{19}$$

is assumed, where $f'(\eta)$ is the original Watson similarity profile and $\delta(x)$ is the nondimensional boundary layer thickness. The profile is then used in a Kármán-

Pohlhausen method of solution. Over Region 1 unretarded fluid is present when $x < x_0$, say where x_0 marks the point of penetration of viscous effects at the free surface, so that $\bar{U}_s(x) = 1$ and $\delta(x) < \bar{h}(x)$ over $0 < x < x_0$. For $x > x_0$ into Region 2 $\delta(x) \equiv \bar{h}(x)$ and $\bar{U}_s(x) < 1$ in a manner which, using the conservation of flow constraint, can be matched directly onto the asymptotic similarity solutions.

The momentum integral equation reads

$$\frac{\mathrm{d}}{\mathrm{d}x}\int_0^{\delta(x)} \bar{U}(1-\bar{U})\,\mathrm{d}y = \left(\frac{\partial \bar{U}}{\partial y}\right)_{y=0} \qquad (20)$$

and using equation (19) leads to the solution

$$\delta^2(x) = \frac{3\sqrt{3}c^3 x}{\pi - c\sqrt{3}}, \qquad (21)$$

where $\delta(x) = 0$ has been assumed at $x = 0$, which is valid in the limit of the underlying assumption.

Invoking the conservation of volume flow at x_0, the end point of Region 1 leads to

$$\int_0^{\delta(x)} \bar{U}\,\mathrm{d}y - (\bar{h} - \delta) = 1 \qquad (22)$$

where

$$\bar{h}(x) = 1 + \left(1 - \frac{2\pi}{3\sqrt{3}c^2}\right)\delta. \qquad (23)$$

Since $\delta(x_0) = \bar{h}$

$$x_0 = \frac{3\sqrt{3}c(\pi - c\sqrt{3})}{4\pi^2} \approx 0.13162 \qquad (24)$$

and matching the free surface velocity at $x = x_0$ leads to

$$l = \frac{3\sqrt{3}c}{4\pi^2}(3\sqrt{3}c - \pi) \approx 0.7646. \qquad (25)$$

Notice that as a result of the choice of approximating profile the velocity distribution at the end of Region 1 exactly matches that of Region 2.

5.2. Alternative profiles

Although the Watson profile may be thought to be the most effective in suppressing the transition region, any convenient profile may be used in the momentum integral equation. When considering the heat transfer characteristics of the flow by means of the

energy integral equation, the use of $f'(\eta)$, which is only known as a numerical solution, is unwieldy. A polynomial approximation to the velocity profile is more convenient.

To maintain the aggregate and matching properties of $f'(\eta)$, and simultaneously exploit the convenience of a polynomial representation, a fourth-order polynomial approximation to $f'(\eta)$ has been obtained as

$$f'_w(\eta) = c\eta + (4-3c)\eta^3 + (2c-3)\eta^4, \qquad (26)$$

where c is the constant 1.402. A remarkably close comparison between the polynomial profile and the similarity solution is illustrated in Fig. 3. For comparison note that

$$\int_0^1 f'(\eta)\,d\eta = \frac{2\pi}{3\sqrt{3c^2}} \approx 0.615 \qquad (27)$$

$$\int_0^1 f'_w(\eta)\,d\eta = \frac{8+3c}{20} \approx 0.6103.$$

The viscous boundary layer thickness for this profile is given by

$$\delta_w^2 = \frac{1260cx}{72+39c-19c^2} \qquad (28)$$

and

$$x_{0_w} = \frac{20(72+39c-19c^2)}{63c(8+3c)^2} \approx 0.13577 \qquad (29)$$

$$l_w = \frac{567c^3(8+3c)^2 - 40\pi^2(72+39c-19c^2)}{126\pi^2 c(8+3c)^2} \approx 0.7604 \qquad (30)$$

which very closely approximate equations (24) and (25). The polynomial $f'_w(\eta)$ is consequently used in subsequent developments of the velocity and temperature distributions.

It remains to establish the temperature characteristics in Region 1. The energy integral equation of (10) becomes

$$\frac{d}{dx}\int_0^{\delta_T(x)} \bar{U}(1-\bar{\phi})\,dy = \frac{1}{Pr}\left(\frac{\partial\bar{\phi}}{\partial y}\right)_{y=0}, \qquad (31)$$

where $\delta_T(x)$ denotes the outer limits of the region of thermal diffusion. For $Pr > 1$, $\delta_T(x) < \delta(x)$ over $0 < x < x_0$. The notation $\eta_T = y/\delta_T(x)$ is introduced and the ratio δ_T/δ is denoted by Δ so that $\eta = \Delta\eta_T$. The solution for $\delta_T(x)$ is again developed by assuming profiles for $\bar{U}$ and $\bar{\phi}$ as

$$\bar{U}(\eta) = f'_w(\eta) \quad \bar{\phi}(\eta_T) = f_w(\eta_T) \qquad (32)$$

which ensures identical velocity and temperature distributions for $Pr = 1$ when also $\Delta = 1$.

Assuming a constant ratio Δ leads to

$$\Delta^2 D(\Delta) = \frac{4(72+39c-19c^2)}{Pr}, \qquad (33)$$

where $D(\Delta) = 168c(3-c)\Delta + 27(4-3c)(5-2c)\Delta^3 - 7(3-2c)(12-5c)\Delta^4$.

The values of Δ, obtained for various Prandtl numbers, are listed in Table 1.

5.3. *Region* 2

In Region 2, the hydrodynamics are governed by the Watson similarity solution where thermal diffusion continues to progress across the film. Accordingly the velocity at the free surface is no longer uniform, but is prescribed in nondimensional terms by equation (15). The film thickness $\bar{h}(x)$ and the viscous boundary layer thickness $\delta(x)$ now coincide as

$$\delta(x) = \bar{h}(x) = \frac{\pi}{\sqrt{3}}(x+l_w). \qquad (34)$$

The energy integral equation (31) remains appropriate. The presence of the free surface limits further viscous penetration and $\delta_T(x) \to \delta(x) = \bar{h}(x)$. In prescribing profiles $\eta_T = y/\delta_T(x)$ may again be utilized, but now $\Delta(x) = \delta_T(x)/\delta(x)$ is no longer constant, and must in fact tend to 1 at the end of Region 2.

The following profiles are introduced into the energy equation :

$$\bar{U}(x,\eta) = \bar{U}_s(x) f'_w(\eta) \quad \bar{\phi}(x,\eta_T) = f'_w(\eta_T). \quad (35)$$

The equation for $\delta_T(x)$ is accordingly

$$\delta_T(x)\frac{d}{dx}[\bar{U}_s(x)D(\Delta)\delta_T(x)] = \frac{2520c}{Pr}. \qquad (36)$$

This resultant first-order equation in Δ^2 may now be integrated with initial data $\Delta(x_{0w}; Pr)$ as far as $\Delta(x_{1w}(Pr); Pr)$ to give

$$\Delta^3[3360c(3-c)+648(4-3c)(5-2c)\Delta^2 - 175(3-2c)(12-5c)\Delta^3] = \frac{50\,400}{cPr}\ln\frac{x+l_w}{x_{1w}+l_w} + 6660 + 2001c - 1222c^2. \qquad (37)$$

x_{1w} marks the end of Region 2, as predicted, using the Watson polynomial profile. Beyond x_{1w} viscous and thermal effects are present throughout the film.

The values of $x_{1w}(Pr)$ are listed in Table 2. The numerical details for various *Pr* are presented in Table 3.

5.4. *Region* 3

The boundary condition of zero heat flux at the edge of the developing thermal layer in Region 1 and Region 2 is based on the assumption of a continuous temperature distribution developing smoothly into the impinging jet temperature. Once the temperature effects of the hot wall penetrate the free surface beyond $x_{1w}(Pr)$ the zero heat flux boundary condition remains appropriate. Here, however, it reflects the insulating role of the surrounding air. As a consequence, the temperature of the film will now rise as a result of continuing heat input at the plate. In fact the temperature of the film will now progress to T_w, so long as the insulating boundary condition is maintained.

To accommodate the adjustment of the film temperature to T_w, the following profiles are adopted

$$\bar{U}(x,\eta) = \bar{U}_s(x) f'_w(\eta) \quad \bar{\phi}(x,\eta) = \beta(x) f'_w(\eta) \quad (38)$$

where now $\eta = y/\bar{h}(x)$.

The energy integral equation now reads

$$\frac{\mathrm{d}}{\mathrm{d}x}\int_0^{\bar{h}(x)} \bar{U}(\beta-\bar{\phi})\,\mathrm{d}y - \int_0^{\bar{h}(x)} \bar{U}\frac{\mathrm{d}\beta}{\mathrm{d}x}\mathrm{d}y = \frac{1}{Pr}\left(\frac{\partial\bar{\phi}}{\partial y}\right)_{y=0}. \quad (39)$$

The result is an equation for $\beta(x)$ within the framework of prescribed film thickness, namely

$$\frac{72+39c-19c^2}{630}\frac{\mathrm{d}}{\mathrm{d}x}(\bar{U}_s\bar{h}\beta) - \frac{8+3c}{20}\bar{U}_s\bar{h}\frac{\mathrm{d}\beta}{\mathrm{d}x} = \frac{c}{Pr}\frac{\beta}{\bar{h}} \quad (40)$$

and hence,

$$\beta(x) = \left(\frac{x_{1w}+l_w}{x+l_w}\right)^{\frac{840}{c(360+111c-38c^2)Pr}} \approx \left(\frac{x_{1w}+l_w}{x+l_w}\right)^{\frac{1.015}{Pr}} \quad (41)$$

which satisfies the requirements $\beta\left(x_{1w}(Pr)\right) = 1$ and has $\beta \to 0$ at rates dependent on *Pr*.

6. APPROXIMATE SOLUTION RESULTS

The approximate solution scheme outlined provides comprehensive details of the flow and heat transfer characteristics for the model flow. Estimates of film thickness, velocity and temperature distributions, skin friction and heat transfer coefficients over the entire region downstream of the point of impingement can be obtained.

A more detailed indication of the region by a region form of solution appears in Fig. 4. For Prandtl numbers Pr = 2, 5 and 10 film thickness profiles incorporating the viscous and thermal diffusion processes to penetration are presented.

The elements of interest in engineering practice are the shear stress at the solid boundary, i.e. the skin friction and the rate of heat transfer at the boundary. The skin friction is defined as

$$\tau = \mu\left(\frac{\partial U}{\partial Y}\right)_{Y=0} \tag{42}$$

leading to the nondimensional skin friction coefficient

$$\bar{\tau} = \frac{H_0\tau}{\mu U_0} = \frac{\tau Re}{\rho U_0^2} = \left(\frac{\partial \bar{U}}{\partial y}\right)_{y=0}. \tag{43}$$

The approximate solutions give

$$\bar{\tau}_w = \sqrt{\frac{(72+39c-19_c^2)c}{1260x}} \text{ in Region 1}$$

$$= \frac{9\sqrt{3}c^3}{2\pi^3(x+l_w)^2} \text{ in Regions 2 and 3.} \tag{44}$$

$\bar{\tau}(x)$ is plotted in Fig. 5. The integrable square root singularity is consistent with the Blasius boundary layer equivalent.

The most significant film cooling design factor is the heat transfer across the film. The heat transfer at the solid boundary is given by

$$q = -k\left(\frac{\partial T}{\partial Y}\right)_{Y=0} = \frac{k\Delta T}{H_0}\left(\frac{\partial \bar{\phi}}{\partial y}\right)_{y=0}, \tag{45}$$

where $\Delta T = T_w - T_0$. The nondimensional version is the Nusselt number defined as

$$Nu = \frac{qH_0}{k\Delta T} = \left(\frac{\partial \bar{\phi}}{\partial y}\right)_{y=0}. \tag{46}$$

The results are

$$Nu_w = \frac{1}{\Delta_w(Pr)}\sqrt{\frac{(72+39c-19c^2)c}{1260x}} \text{ in Region 1}$$

$$= \frac{1}{\Delta_w(x;Pr)}\frac{\sqrt{3c}}{\pi(x+l_w)} \text{ in Region 2}$$

$$= \frac{\sqrt{3c}}{\pi(x+l_w)}\left(\frac{x_{1w}+l_w}{x+l_w}\right)^{\frac{840}{c(360+111c+38c^2)Pr}}$$

in Region 3. (47)

The predictions of Nu_w, for a range of Prandtl numbers are presented in Fig. 6. The values of $\Delta_w(Pr)$ have been obtained from equation (33) and $\Delta_w(x;Pr)$ is the solution of equation 37.

7. NUMERICAL SOLUTION

The approximate solution so far developed is based on a qualitative appraisal of the anticipated hydrodynamic and thermal features of the jet flow. However, there is no means of assessing the validity or accuracy of the solution other than by direct numerical solution of the overall differential system. Such an assessment is essential if the methodology is to be carried over with confidence into more complex settings, such as cylinder inundation.

The numerical problem is the solution of the system

$$\frac{\partial^3\psi}{\partial y^3} = \frac{\partial\psi}{\partial y}\frac{\partial^2\psi}{\partial x\partial y} - \frac{\partial\psi}{\partial x}\frac{\partial^2\psi}{\partial y^2} \tag{48}$$

$$\frac{\partial^2\bar{\phi}}{\partial y^2} = Pr\left(\frac{\partial\psi}{\partial y}\frac{\partial\bar{\phi}}{\partial x} - \frac{\partial\psi}{\partial x}\frac{\partial\bar{\phi}}{\partial y}\right) \tag{49}$$

subject to the boundary conditions

$$\psi = 0 \quad \frac{\partial\psi}{\partial y} = 0 \quad \bar{\phi} = 0 \quad \text{on } y = 0 \quad x \geqslant 0 \tag{50}$$

$$\psi = 1 \quad \frac{\partial^2\psi}{\partial y^2} = 0 \quad \frac{\partial\bar{\phi}}{\partial y} = 0 \quad \text{at } y = \bar{h}(x) \quad x \geqslant 0 \tag{51}$$

$$\bar{h} = 1 \quad \psi = y \quad \bar{\phi} = 1 \quad \text{at } x = 0 \quad 0 < y \leqslant 1, \tag{52}$$

where equation (52) is the essential initial condition for the parabolic system reflecting conditions at jet deflection.

The solution algorithm is a development of that of Hunt [14], who considered the numerical solution of parabolic free boundary problems for isothermal thin film flows. In anticipation of the use of a Keller box method and its attractive extrapolation features, the differential system is re-cast as the following first-order system :

$$\frac{\partial \psi}{\partial y} = \bar{u} \quad \frac{\partial \bar{u}}{\partial y} = \bar{v} \quad \frac{\partial \bar{v}}{\partial y} = \bar{u}\frac{\partial \bar{u}}{\partial x} - \bar{v}\frac{\partial \psi}{\partial x} \tag{53}$$

$$\frac{\partial \bar{\phi}}{\partial y} = \bar{w} \quad \frac{\partial \bar{w}}{\partial y} = Pr\left(\bar{u}\frac{\partial \bar{\phi}}{\partial x} - \bar{w}\frac{\partial \psi}{\partial x}\right) \tag{54}$$

whose boundary conditions are

$$\begin{aligned} &\psi = 0 \quad \bar{u} = 0 \quad \bar{\phi} = 0 \quad \text{on } y = 0 \quad 0 \leqslant x < +\infty \\ &\psi = 1 \quad \bar{v} = 0 \quad \bar{w} = 0 \quad \text{on } y = \bar{h}(x), 0 \leqslant x < +\infty \\ &\bar{h} = 1 \quad \psi = y \quad \bar{\phi} = 1 \quad \text{on } x = 0 \quad 0 < y \leqslant 1. \end{aligned} \tag{55}$$

Hunt ingeniously introduces the following coordinate transformation that simultaneously maps the film thickness onto the unit interval and removes the Blasius singularity at the origin :

$$x = \xi^2, \quad y = \frac{\xi \eta \bar{h}}{\xi + 1 - \eta}. \tag{56}$$

In the spirit of the continuous transformation algorithm of Hunt and Wilks [15], these are supplemented by transformations of the dependent variables which incorporate the growth rates of their asymptotic behaviour as known from the downstream similarity solutions. As a result, all dependent variable remain of order unity over all ξ. The appropriate transformations are

$$\begin{aligned} &\psi(x, y) = \frac{\xi}{\xi + 1 - \eta} f(\xi, \eta) \quad \bar{u}(x, y) = \frac{u(\xi, \eta)}{(1 + \xi)^2} \\ &\bar{v}(x, y) = \frac{\xi + 1 - \eta}{\xi(1 + \xi)^4} v(\xi, \eta), \quad \bar{\phi}(x, y) = \phi(\xi, \eta) \\ &\bar{w}(x, y) = \frac{\xi + 1 - \eta}{\xi(1 + \xi)^2} w(\xi, \eta) \quad \bar{h}(x) = (1 + \xi)^2 h(\xi). \end{aligned} \tag{57}$$

The equations to be solved now read

$$f_\eta = \frac{(1+\xi)hu}{\xi+1-\eta} - \frac{f}{\xi+1-\eta} \tag{58}$$

$$u_\eta = \frac{(1+\xi)hv}{\xi+1-\eta} \tag{59}$$

$$v_\eta = \frac{v}{\xi+1-\eta} - \frac{\xi(1+\xi)^2 hu^2}{(\xi+1-\eta)^3} - \frac{(1-\eta)(1+\xi)^3 hfv}{2(\xi+1-\eta)^4} + \frac{\xi(1+\xi)^3 h}{2(\xi+1-\eta)^3}(uu_\xi - vf_\xi) \tag{60}$$

$$\phi_\eta = \frac{(1+\xi)hw}{\xi+1-\eta} \tag{61}$$

$$w_\eta = \frac{w}{\xi+1-\eta} - \frac{Pr(1-\eta)(1+\xi)^3 hfw}{2(\xi+1-\eta)^4} + \frac{Pr\xi(1+\xi)^3 h}{2(\xi+1-\eta)^3}(u\phi_\xi - wf_\xi) \tag{62}$$

subject to

$$\begin{aligned} &f = 0 \quad u = 0 \quad \phi = 0 \quad \text{on } \eta = 0 \quad 0 \leqslant \xi + \infty \\ &f = 1 \quad v = 0 \quad w = 0 \quad \text{on } \eta = 1 \quad 0 \leqslant \xi < +\infty \\ &h = 1 \quad f = f_0(\eta) \quad \phi = \phi_0(\eta) \quad \text{at } \xi = 0 \quad 0 < \eta \leqslant 1, \end{aligned} \tag{63}$$

where $f_0(\eta), \phi_0(\eta)$ are found by putting $\xi = 0$, $h = 1$ into equations (58)−(62) and solving, subject to conditions $f = u = \phi = 0$ at $\eta = 0$ and $u = 1$, $\phi = 1$ at $\eta = 1$.

The parabolic system of equations and boundary conditions (58)−(63) has been solved by marching in the ξ-direction using a modification of the Keller box method. A nonuniform grid is placed on the domain $\xi \geqslant 0$, $0 \leqslant \eta \leqslant 1$, and the resulting difference equations are solved by Newton iteration. Solutions are obtained on different sized grids and Richardson's extrapolation used to produce results of high accuracy. A full account of the numerical method and the details of implementation is beyond the scope of this paper and will be reported separately. The solution scheme was successfully tested against previously reported results.

8. NUMERICAL RESULTS AND COMPARISONS

A typical run had a coarse grid of dimension 60 × 48 on the (ξ, η) domain with each cell being divided into 1, 2, 3 and 4 sub-cells, respectively. Because of the coordinate

singularity at $\xi = 0$, $\eta = 1$ a nonuniform grid was employed given by $\xi = 1/3 \sinh [\bar{\xi}^{1.5}(1 + \bar{\xi}^{1.5})]$, $\eta = 1 - (1 - \bar{\eta})^{1.5}$, where $\bar{\xi}$ and $\bar{\eta}$ are uniform. When $\Delta\bar{\xi} \equiv 0.044618955$ and $\Delta\bar{\eta} \equiv 1/47$, this gave $\Delta\xi \sim 0.004$ and $\Delta\eta \sim 0.003$ near the singularity, which is sufficiently small to give good accuracy, and this enabled us to integrate as far as $\xi \sim 10^9$, which was necessary for the profile at infinity to be determined with sufficient accuracy. From the convergence of the extrapolation process the absolute error is 3×10^{-7}. A typical set of numerical data is presented in Table 4.

In Fig. 7, the film thickness profiles obtained from both the numerical and approximate solutions are compared and in Fig. 8 the comparison is repeated for free surface velocities. In each case there is good agreement between the respective solutions for these aggregate hydrodynamic properties. Figure 9 presents a comparison of predicted velocity profiles at various downstream stations. An excellent agreement in boundary data at the plate is achieved, as indicated in the display of skin friction estimates in Fig. 10.

The comparison of thermal characteristics appear in Figs. 11−13. In Fig. 11 the results for free surface temperature estimates are compared for a selection of Prandtl numbers (2, 5 and 10), whilst Fig. 12 compares temperature distributions at downstream stations along the plate. Figure 13 once again displays excellent agreement in boundary data in the form of comparisons of local heat transfer coefficients at various Prandtl numbers.

9. CONCLUDING REMARKS

An approximate and an exact numerical solution for the flow of a cold two-dimensional jet against a hot, horizontal plate have been presented. There is good overall agreement between the approximate and numerical solutions. The elements of engineering practice, namely the skin friction and heat transfer coefficients, show excellent agreement. Although at this stage a comparison between theory and experiment is unavailable, every indication is that the approximate solution may be carried over with confidence to the cylinder inundation problem, thus providing a basis of comparison with Mitrovic's experimental results. The work also provides the basis for re-assessing condensation drainage and inundation flows ; recognizing that in contrast to Nusselt theory, the inertia of the inundating film may generate significant heat transfer at the top of a flooded cylinder. In particular such an implementation of the present approximate method is likely to yield significant heat transfer at the top of an inundated cylinder. This is in contrast to models based solely on a balance of viscous and gravitational terms, which necessarily predict zero heat transfer at the upper generator.

REFERENCES

1. Z. H. Chaudhury, Heat transfer in a radial liquid jet, *J. Fluid Mech.* **20**, 501−511 (1964).
2. P. M. Brdlik and V. K. Savin. Heat transfer between an axisymmetric jet and a plate normal to the flow, *J. Engng Phys.* **8**, 91−98 (1965).
3. N. R. Saad, W. J. M. Douglas and A. S. Mujumdar, Prediction of heat transfer under an axisymmetric laminar impinging jet, *Ind. Engng Chem. Fundam.* **16**, 148−154 (1977).
4. A. W. Lipsett and R. R. Gilpin, Laminar jet impingement heat transfer including the effects of melting, *Int. J. Heat Mass Transfer* **21**, 25−33 (1978).
5. X. S. Wang, Z. Dagan and L. M. Jiji, Heat transfer between a circular free impinging jet and a solid surface with non-uniform wall temperature or wall heat flux−1. Solution for the stagnation region, *Int. J. Heat Mass Transfer* **32**, 1351−1360 (1989).
6. X. S. Wang, Z. Dagan and L. M. Jiji, Heat transfer between a circular free impinging jet and a solid surface with non-uniform wall temperature or wall heat flux−2. Solution for the boundary layer region, *Int. J. Heat Mass Transfer* **32**, 1361−1371 (1989).
7. E. J. Watson, The radial spread of a liquid jet over a horizontal plane, *J. Fluid Mech.* **20**, 481-499 (1964).
8. A. Solan and A. Zfati, Heat transfer in laminar flow of a liquid film on a horizontal cylinder, *Heat Transfer* 1974, *Proceedings of the Fifth International Heat Transfer Conference*, Keidanrenkaikan Building, Tokyo, Japan. Vol. II, pp. 90−93 (1974).
9. W. H. Parken and L. S. Fletcher, Heat transfer in thin liquid films flowing over horizontal tubes, *Proceedings of the Sixth International Heat Transfer Conference*, Toronto, Canada, pp. 415−420 (1978).
10. J. T. Rogers, Laminar falling film flow and heat transfer characteristics on horizontal tubes, *Can. J. Chem. Engng* **59**, 213−222 (1981).
11. J. W. Andberg and G. C. Vliet, Absorption of vapors into liquid films flowing over cooled horizontal tubes, *Heat Transfer* 1986, *Proceedings of the Eighth International Heat Transfer Conference,* San Francisco, CA (1986).
12. J. Mitrovic, Influence of tube spacing and flow-rate on heat-transfer from a horizontal tube to a falling liquid-film, *The 8th International Conference on Heat Transfer,* San Francisco, CA (1986).
13. M. A. Abdelghaffer, A. A. Nicol, R. J. Gribben and G. Wilks, Thin film inundation flow over a horizontal cylinder, *Math. Engng Ind.* **2**,143−155 (1989).
14. R. Hunt, The numerical solution of parabolic free boundary problems arising from thin film flows, *J. Comput. Phys.* **84,** 377−402 (1989).
15. R. Hunt and G. Wilks, Continuous transformation computation of boundary layer equations between similarity regimes, *J. Computat. Phys.* **40,** 478−490. (1981).

List of Table

List of Figures

Pr	Δ
1.0	1.0000
2.0	0.7878
3.0	0.6863
4.0	0.6227
5.0	0.5775
6.0	0.5431
7.0	0.5157
8.0	0.4931
9.0	0.4740
10.0	0.4575

Table 1

Pr	$x_{1w}(Pr)$
1.0	0.1358
2.0	0.3292
3.0	0.5654
4.0	0.8528
5.0	1.2030
6.0	1.6291
7.0	2.1476
8.0	2.7787
9.0	3.5468
10.0	4.4821

Table 2

$\frac{x - x_{0w}}{x_{1w} - x_{0w}}$	$\Delta(x) Pr = 2$	$Pr = 5$	$Pr = 10$
0.0	0.7878	0.5775	0.4575
0.1	0.8161	0.6725	0.6623
0.2	0.8421	0.7403	0.7562
0.3	0.8663	0.7931	0.8166
0.4	0.8888	0.8364	0.8606
0.5	0.9100	0.8729	0.8949
0.6	0.9300	0.9046	0.9229
0.7	0.9488	0.9324	0.9464
0.8	0.9667	0.9573	0.9666
0.9	0.9838	0.9796	0.9843
1.0	1.0000	1.0000	1.0000

Table 3

x	Film thickness $\bar{h}(x)$	Free surface velocity $\bar{u}(x, \bar{h}(x))$	Free surface temperature $\bar{\phi}(x, \bar{h}(x))$
0.000	1.000	1.000	1.000
1.171×10^{-2}	1.186	1.000	1.000
5.151×10^{-2}	1.391	0.998	1.000
0.197	1.768	0.904	0.987
0.567	2.458	0.661	0.878
1.233	3.667	0.443	0.724
1.874	4.830	0.337	0.631
4.650	9.864	0.165	0.441
12.853	24.745	6.571×10^{-2}	0.278
40.118	74.199	2.191×10^{-2}	0.160
1.429×10^{2}	2.607×10^{2}	6.238×10^{-3}	8.517×10^{-2}
5.866×10^{2}	1.065×10^{3}	1.526×10^{-3}	4.204×10^{-2}
2.798×10^{3}	5.077×10^{3}	3.203×10^{-4}	1.923×10^{-2}
1.564×10^{4}	2.838×10^{4}	5.730×10^{-5}	8.128×10^{-3}
1.034×10^{5}	1.875×10^{5}	8.672×10^{-6}	3.161×10^{-3}
2.544×10^{7}	4.614×10^{7}	3.524×10^{-8}	2.014×10^{-4}
1.236×10^{9}	2.242×10^{9}	7.251×10^{-10}	2.890×10^{-5}
1.228×10^{13}	2.227×10^{13}	7.300×10^{-14}	3.000×10^{-7}
1.000×10^{18}	1.814×10^{18}	8.964×10^{-19}	0.000

Table 4

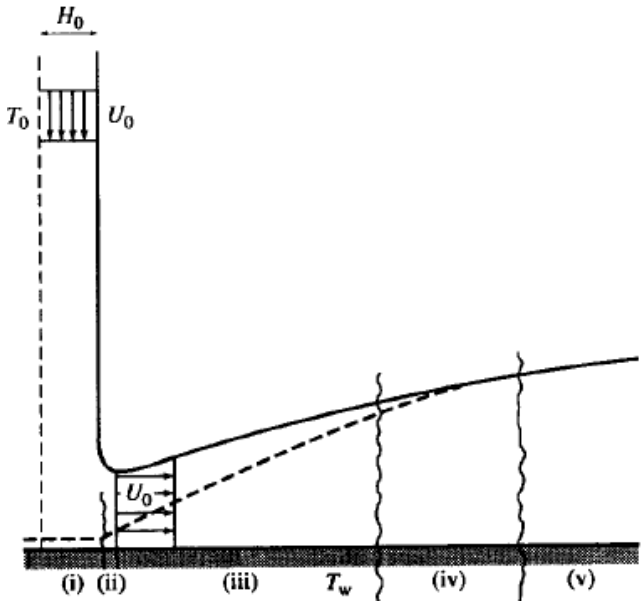

Fig. 1

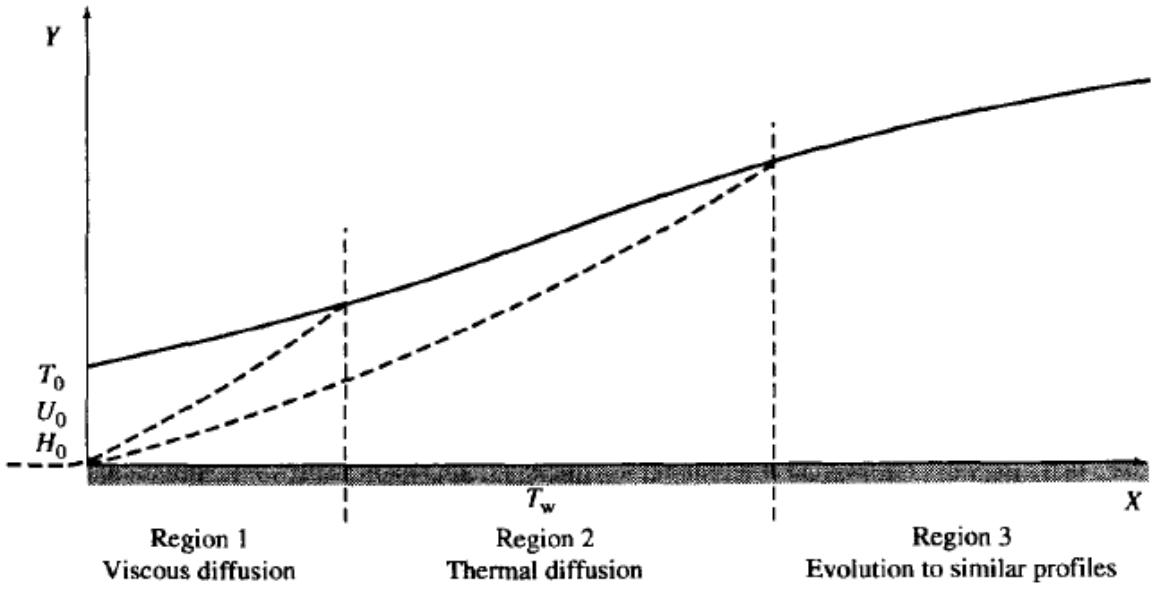
Y
T_0
U_0
H_0
T_w
X
Region 1
Viscous diffusion
Region 2
Thermal diffusion
Region 3
Evolution to similar profiles

Fig. 2

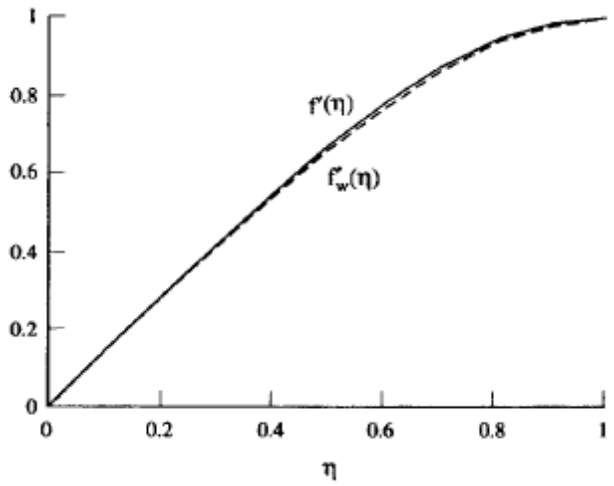

Fig. 3

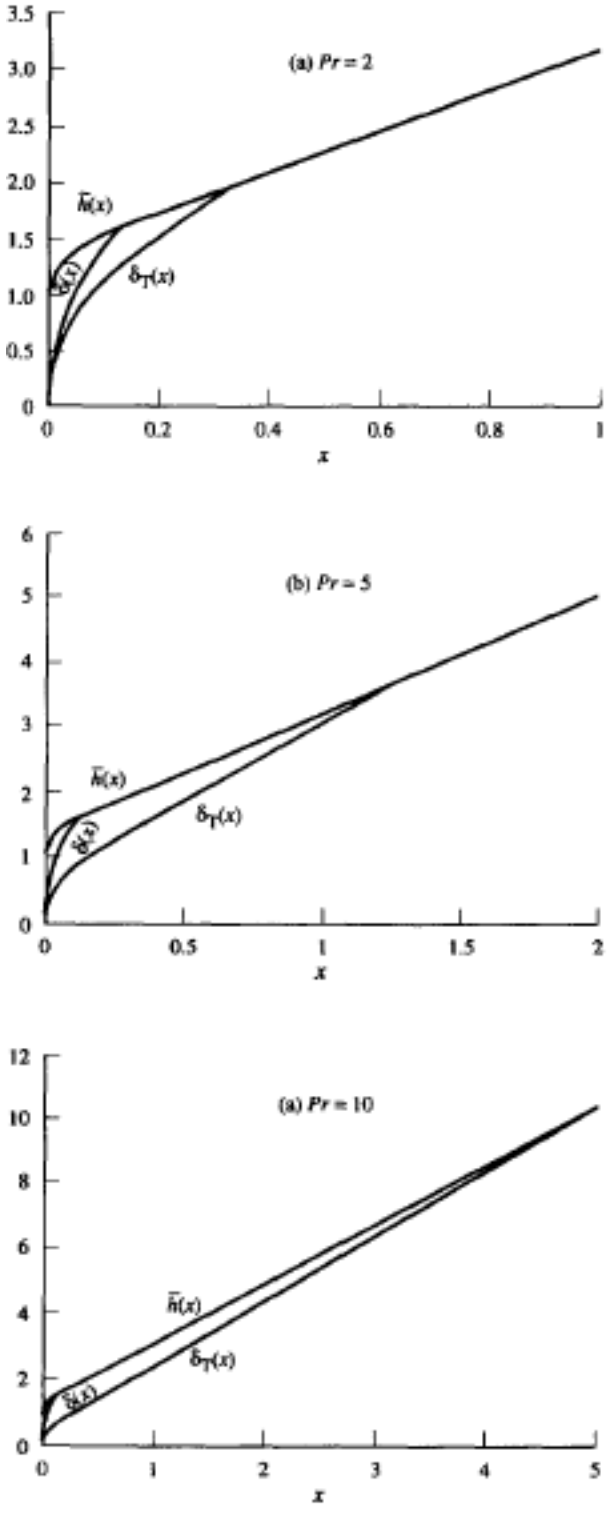
(a) Pr = 2
$\bar{h}(x)$
$\delta(x)$
$\delta_T(x)$
x
(b) Pr = 5
$\bar{h}(x)$
$\delta(x)$
$\delta_T(x)$
x
(a) Pr = 10
$\bar{h}(x)$
$\delta_T(x)$
$\delta(x)$
x

Fig. 4

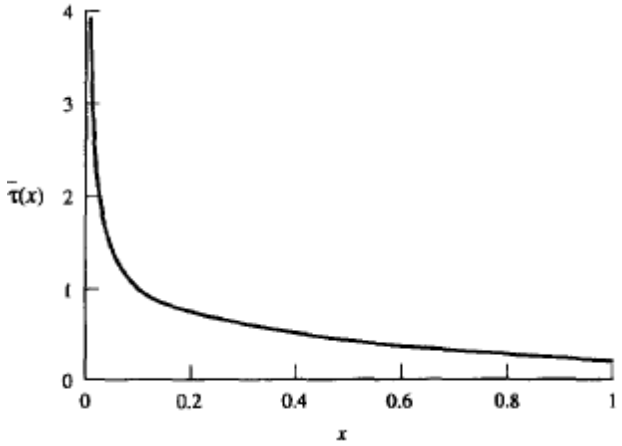

Fig. 5

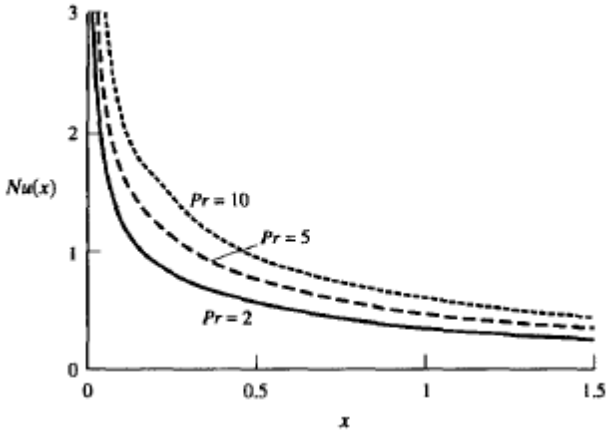

Fig. 6

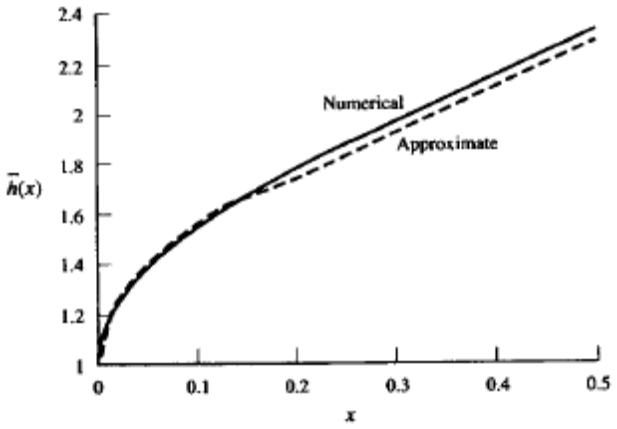
2.4
2.2
2
1.8
1.6
1.4
1.2
1
$\bar{h}(x)$
Numerical
Approximate
0
0.1
0.2
0.3
0.4
0.5
x

Fig. 7

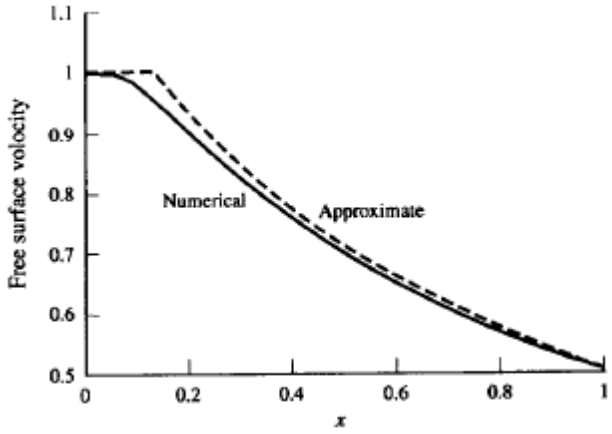
1.1
1
0.9
0.8
0.7
0.6
0.5
Free surface velocity
Numerical
Approximate
0
0.2
0.4
0.6
0.8
1
x

Fig. 8

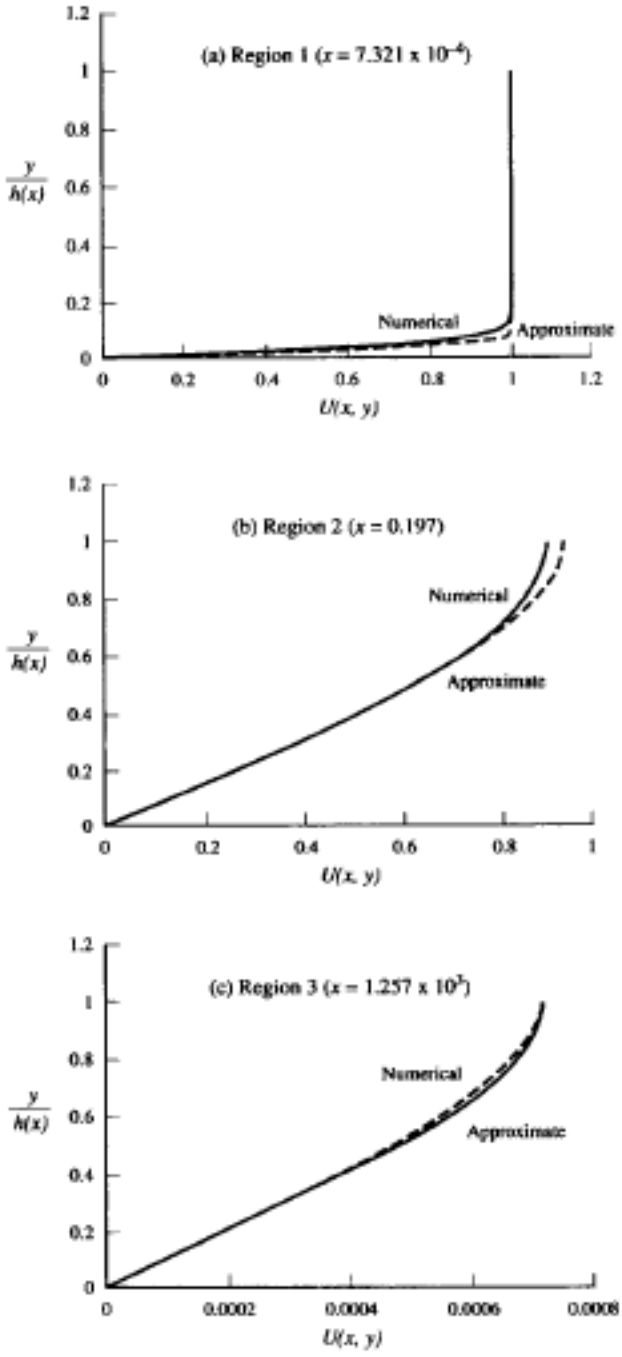
(a) Region 1 ($x = 7.321 \times 10^{-4}$)
$\frac{y}{h(x)}$
Numerical
Approximate
$U(x, y)$
(b) Region 2 ($x = 0.197$)
Numerical
Approximate
(c) Region 3 ($x = 1.257 \times 10^{1}$)
Numerical
Approximate

Fig. 9

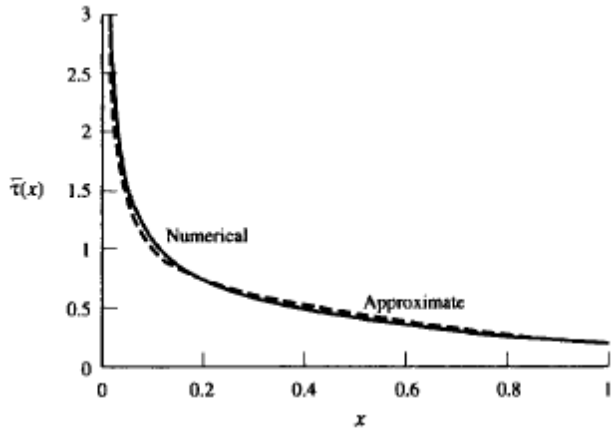

Fig. 10

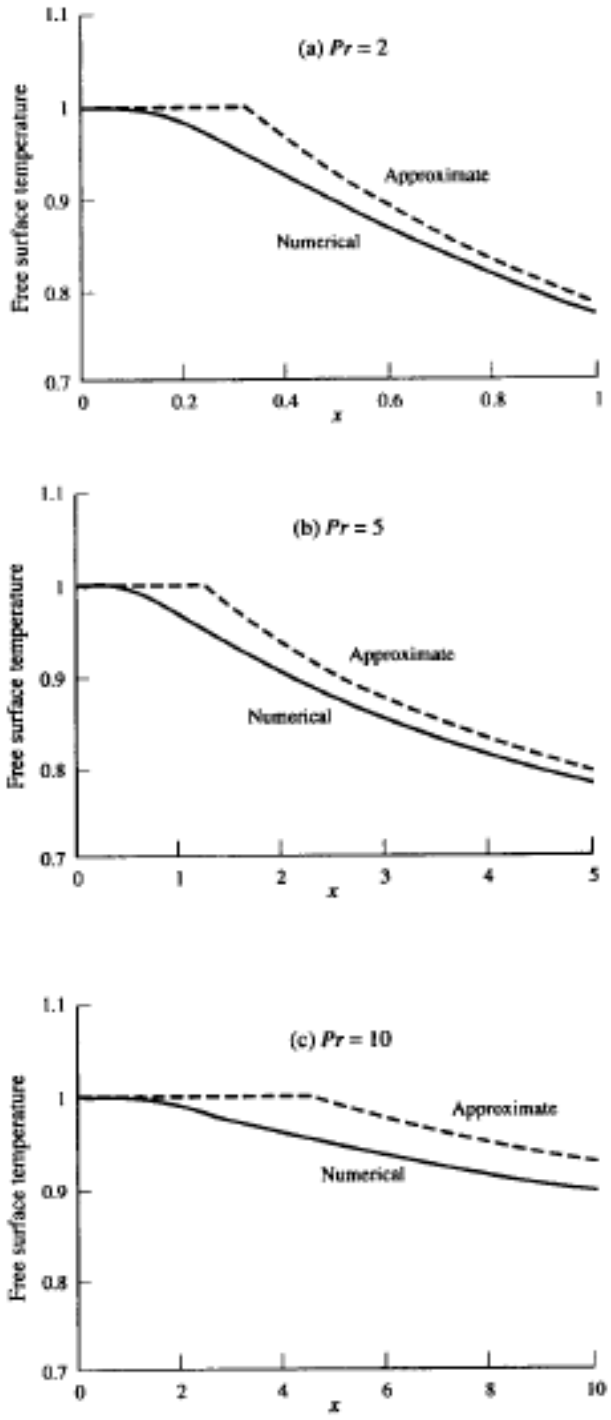
(a) Pr = 2
Free surface temperature
Approximate
Numerical
x
(b) Pr = 5
Free surface temperature
Approximate
Numerical
x
(c) Pr = 10
Free surface temperature
Approximate
Numerical
x

Fig. 11

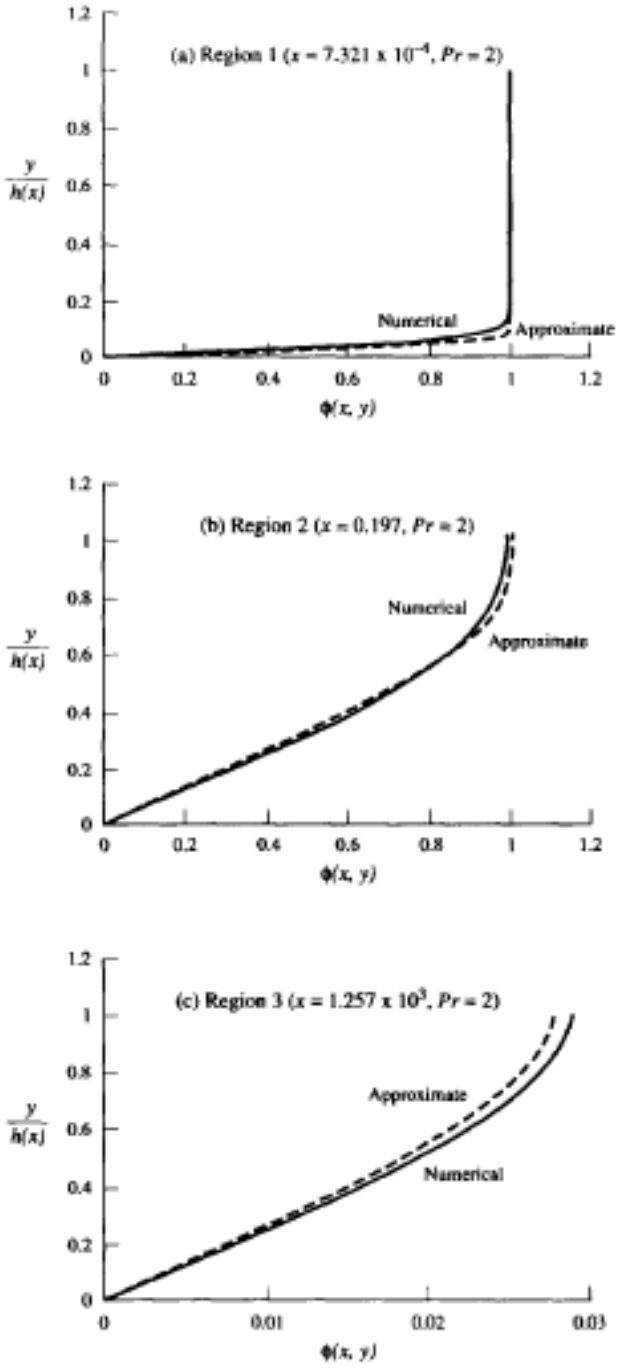
(a) Region 1 ($x = 7.321 \times 10^{-4}$, $Pr = 2$)
Numerical
Approximate
$\frac{y}{h(x)}$
$\phi(x, y)$
(b) Region 2 ($x = 0.197$, $Pr = 2$)
Numerical
Approximate
$\frac{y}{h(x)}$
$\phi(x, y)$
(c) Region 3 ($x = 1.257 \times 10^{3}$, $Pr = 2$)
Approximate
Numerical
$\frac{y}{h(x)}$
$\phi(x, y)$

Fig. 12

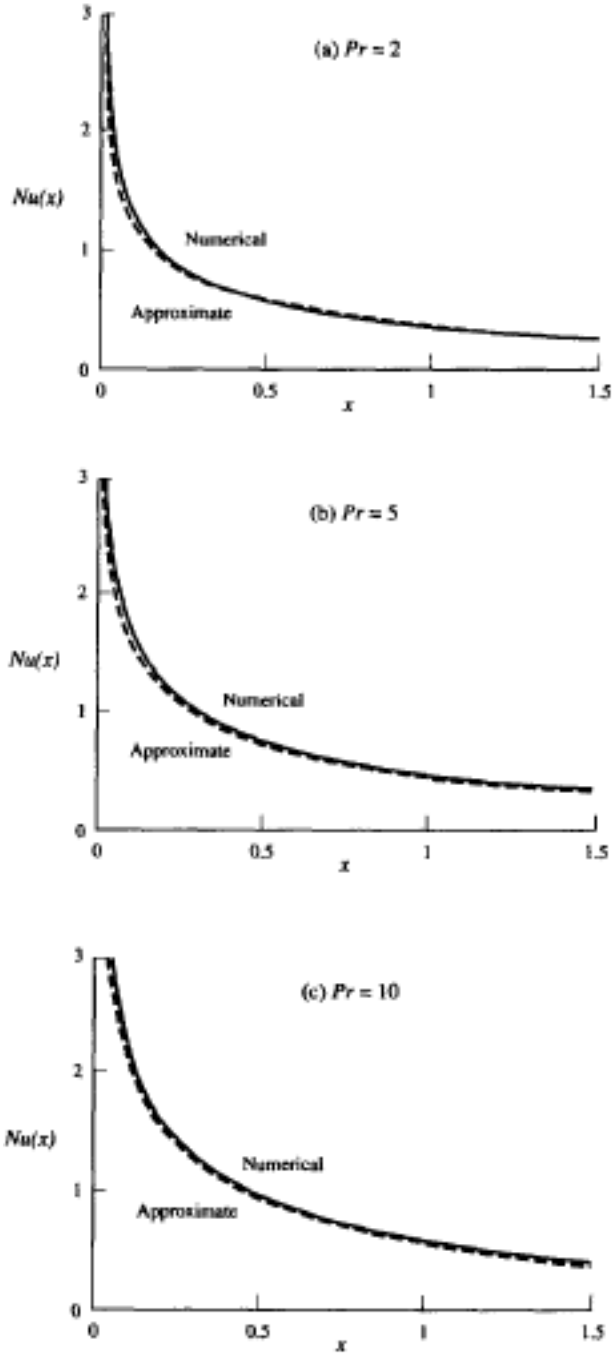
(a) Pr = 2
Nu(x)
Numerical
Approximate
x
(b) Pr = 5
Nu(x)
Numerical
Approximate
x
(c) Pr = 10
Nu(x)
Numerical
Approximate
x

Fig. 13